Physics of Local Optimization in Complex Disordered Systems

Mutian Shen,[1,2] Gerardo Ortiz,[3,4] Zhiqiao Dong,[5] Martin Weigel,[6,7] and Zohar Nussinov[1,6,8,9,*]
[1]Department of Physics, Washington University, St. Louis, Missouri 63160, USA
[2]Department of Biomedical Engineering, Washington University, St. Louis, Missouri 63160, USA
[3]Department of Physics, Indiana University, Bloomington, Indiana 47405, USA
[4]Institute for Advanced Study, Princeton, New Jersey 08540, USA
[5]Department of Mechanical Science and Engineering, University of Illinois Urbana-Champaign, Urbana, Illinois 61801, USA
[6]Institut für Physik, Technische Universität Chemnitz, 09107 Chemnitz, Germany
[7]Physics Department, Emory University, Atlanta, Georgia, USA
[8]Rudolf Peierls Centre for Theoretical Physics, University of Oxford, Oxford OX1 3PU, United Kingdom
[9]LPTMC, CNRS-UMR 7600, Sorbonne Université, 4 Place Jussieu, 75252 Paris cedex 05, France

(Received 1 June 2025; accepted 16 July 2026; published 14 October 2026)

Limited resources motivate decomposing large-scale problems into smaller, "local" subsystems and stitching together the so-found solutions. We explore the physics underlying this approach and discuss the concept of "local hardness," i.e., the complexity of predicting local properties of the solution from local information, for the ground-state problem of both P- and NP-hard spin glasses and related frustrated spin systems. Depending on the model considered, we observe varying scaling behaviors in how errors associated with local predictions decay as a function of the size of the solved subsystem. These errors are intimately connected to global critical threshold instabilities, characterized by gapless, avalanchelike excitations that follow scale-invariant size distributions. Away from criticality, local solvers quickly achieve high accuracy, aligning closely with the results of the computationally much more expensive global minimization. We leverage these findings to introduce a heuristic contraction-based algorithm for globally studying spin-glass ground states. The local solvers further display sharp imprints of the phase transition from the spin-glass to the ferromagnetic phase as the distribution of spin-glass couplings is shifted, as well as characteristic differences for the infinite-range model, implying the existence of specific classes of local hardness. Our findings shed light on how nature may operate solely through local actions at her disposal.

DOI: 10.1103/kcbw-6zkv

A prevalent, "divide-and-conquer" type, approach to analyzing large-scale problems involves segmenting them into smaller "local" components which are then solved, followed by assembling the obtained local optimal solutions in a manner akin to a jigsaw puzzle, thereby yielding meaningful results for the original large-scale problem. This *modus operandi* is natural when constrained by limited time and computational resources. It is especially common when one assumes—as often happens in problems with an underlying geometric structure (e.g., images of physical systems [1] or proteins [2])—that these local solutions provide correct and useful information about the larger system. Such local few-body solvers may accurately capture key features of general many-body systems governed by local Hamiltonians, a result known in certain contexts as nearsightedness [3–7]. Here, we explore physical aspects of this approach for predicting local as well as global aspects of ground states (GSs) of both short- and long-range classical spin-glass systems, a known difficult problem [8,9] using simple local algorithms.

Similar to other complex systems [10–14], the challenge posed by spin glasses results from the combination of disorder and frustration leading to a complex free-energy landscape [15]. According to recent results, these systems generically have very low-lying excited states that are radically different from each other and from the GSs [16–18]. This phenomenon of system-spanning lowest-energy excitations implies that optimal (i.e., GS) subsystem solutions might not necessarily match the optimal full system solution. The occurrence of such excitations is independent of the classification of the corresponding GS problem in the P or NP classes [19]. Indeed, spin glasses with GSs of polynomial (P) complexity may also exhibit system-spanning lowest-energy droplets [18]. This is the case for GSs of two-dimensional (2D) Ising spin glasses on planar graphs, which can be found in polynomial time [20].

Here, we investigate the extent to which local (i.e., subsystem) spin-glass solvers approximate global spin-glass

*Contact author: zohar@wustl.edu

Published by the American Physical Society under the terms of the Creative Commons Attribution 4.0 International license. Further distribution of this work must maintain attribution to the author(s) and the published article's title, journal citation, and DOI.

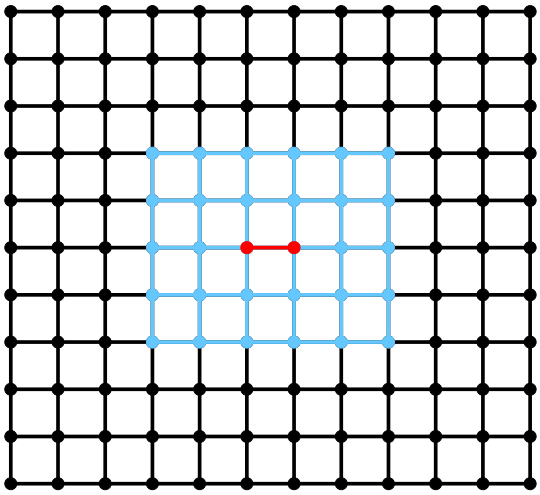


FIG. 1. Computational setup for determining the relative spin orientation $\sigma_{i_0}\sigma_{j_0}$ across the central bond (shown in red). The correct value of $\sigma_{i_0}\sigma_{j_0}$ is that within the GS of the entire system (comprised of black, light blue, and red bonds). The LSBS computes $\sigma_{i_0}\sigma_{j_0}$ within the GS of the local subsystem (light blue and red bonds).

GSs. Understanding such features will help uncover the principles that underlie the effectiveness of local solvers. Our numerical analysis (based on exact GS algorithms) concentrates on Ising spin glasses with Hamiltonian

$$H = -\sum_{\langle ij \rangle} J_{ij}\sigma_i\sigma_j, \qquad \sigma_i = \pm 1, \tag{1}$$

with couplings J_{ij} drawn from a Gaussian distribution of mean $\bar{J}$ and unit variance. Unless stated otherwise, we set $\bar{J} = 0$. Here, the N spins are placed on 2D or 3D lattices with open boundaries and nearest-neighbor interactions [Edwards-Anderson (EA) model [21]] or form a Sherrington-Kirkpatrick (SK) model [22] featuring all-to-all interactions (in which case we rescale J_{ij} by $1/\sqrt{N}$ to guarantee a meaningful thermodynamic limit).

Previous related studies attempted to combine multiple local solvers to address global optimization problems [23], fuse local GSs for the construction of global spin-glass instances with planted solutions [24], and develop local spin-glass solvers using gauge-transformation-based deep reinforcement learning [25,26]. Here, we take on a different perspective and directly investigate the extent to which one can predict (parts of) the global GSs based on optimization of local subsystems. As a minimal realization of this task we study pairs of neighboring spins (bonds) of the model and introduce a "local single-bond solver" (LSBS) that examines neighboring spins within a local subsystem. We first focus on the GS products $\sigma_{i_0}\sigma_{j_0}$ for bonds $\langle i_0 j_0 \rangle$ which, in the simplest case, are located at the center of the system, cf. Fig. 1.

We are interested to see whether the value of this spin product in the global GS matches that obtained by the LSBS for a subsystem centered on this single bond. Recent studies [27] examined correlations between adjacent spins at the system center after resampling its "shell." By contrast, here we examine whether this product, as determined by (i) GS computations for small subsystems containing this bond and using open boundaries, agrees with that in (ii) the global system GS. In this way, the LSBS solves a maximally local problem and hence is a diagnostic tool, leading to our definition of "local hardness." As we shall show below, however, these local solutions can be meaningfully stitched together to form candidate solutions for the full problems by a contraction-based scheme. We will find that system-spanning, correlated changes to spin-glass GSs appear only at special critical interaction strengths [18]. When the spin-glass couplings are far removed from their critical threshold values, at which global avalanchelike changes occur, the GSs are robust to small variations of the coupling constants. This robustness enables the LSBS to become accurate whenever coupling constants are far from their critical values. We find that for large lattice systems, the LSBS error rate becomes independent of the global system size and exhibits a power-law decay with subsystem size. Several other distance-dependent quantities also exhibit power-law behaviors (see Ref. [28], S10). By contrast, the dependence of the LSBS error rate on the deviations of the coupling from its critical value is of an exponential form.

To systematically study the relation of local and global solutions in spin systems, we rely on exact (combinatorial) GS algorithms, using a minimum-weight perfect matching (MWPM) method [36] based on Blossom V [37] for the polynomial 2D problem and the general-purpose Gurobi software [38] for 3D systems and the SK model. Figure 1 schematically depicts the setup: we computed GSs for the entire (N-spin) systems as well as for subsystems with N_{sub} lattice sites centered on the considered bond $\langle i, j \rangle$ (corresponding to the LSBS), comparing the predicted values of the product $\sigma_{i_0}\sigma_{j_0}$ (open boundary conditions are applied in both cases). If the results agree, the bond product is predicted correctly (with zero error). For $L \times L$ square lattices of sizes $L = 256$, 512, 1024, we examined $L_{\mathrm{sub}} \times L_{\mathrm{sub}}$ subsystems with $4 \le L_{\mathrm{sub}} \le 512$, using ~60 000 disorder realizations. For cubic lattices of side lengths $L = 10$ and 12, the $L_{\mathrm{sub}} \times L_{\mathrm{sub}} \times L_{\mathrm{sub}}$ subsystems were of size $4 \le L_{\mathrm{sub}} \le 10$, and we used ~2 000 realizations. From these calculations we estimate the LSBS error rate $\mathcal{E}$. Figure 2 shows the dependence of $\mathcal{E}$ on the subsystem size for several cases. For the lattice systems with $\bar{J} = 0$ we find that, although the 2D and 3D spin-glass GS problems belong to different complexity classes (P and NP, respectively), in both cases the error rate is well described by a power-law decay in the subsystem size [39] [40], namely,

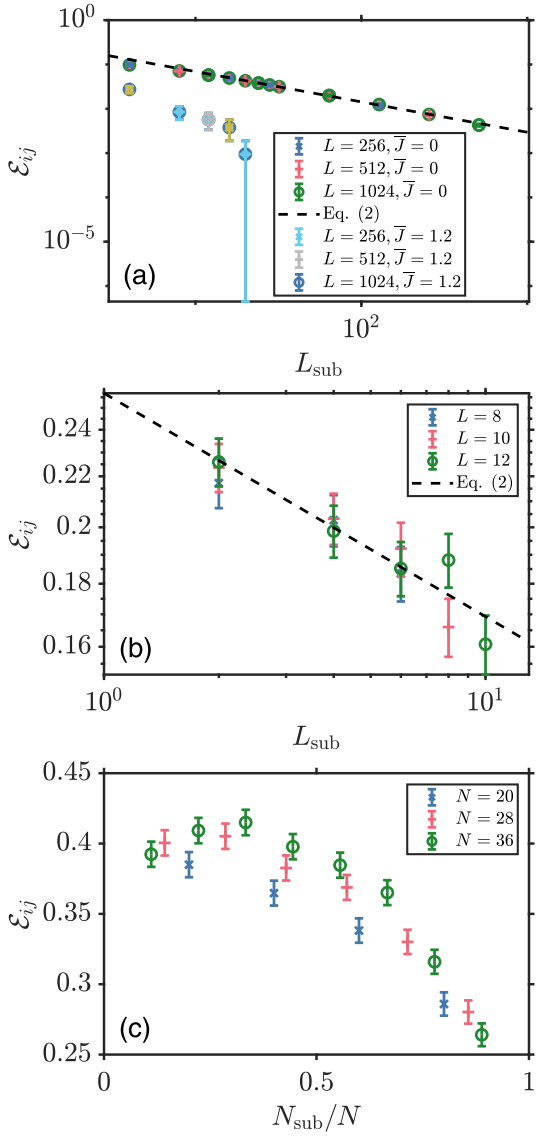


FIG. 2. The disorder-averaged LSBS error rate $\mathcal{E}_{ij}$ as a function of the subsystem size $L_{\rm sub}$ (resp. $N_{\rm sub}$) for (a) the square-lattice (2D) EA model, (b) the cubic lattice (3D) EA model, and (c) the SK model. For each plot, the results for varying system sizes L (N) are shown. For (a), both cases $\bar{J} = 0$ and $\bar{J} = 1.2$ are shown, whereas in (b) and (c) $\bar{J} = 0$. Note the nearly perfect collapse of different system-size data, indicating that the error of the LSBS becomes asymptotically independent of system size for (a) and (b), while this is only the case if one scales $N_{\rm sub}$ with N for the SK model in (c). For the lattice systems in (a), (b) and $\bar{J} = 0$, the error rate is fit by Eq. (2), cf. the straight dashed lines.

$$\mathcal{E}_{ij} \equiv \frac{1 - [\sigma_i \sigma_j \sigma_i^{\rm sub} \sigma_j^{\rm sub}]}{2} \sim (\ell_{\mathcal{E}}/L_{\rm sub})^{\kappa}. \tag{2}$$

Here, $[\sigma_i \sigma_j \sigma_i^{\rm sub} \sigma_j^{\rm sub}]$ denotes the pair-overlap correlation function, where $[\cdots]$ represents the disorder average, and $\ell_{\mathcal{E}}$ is an effective length scale. Importantly, this algebraic decay is independent of the linear system size L, cf. the data collapse in Figs. 2(a) and 2(b). Comparing the respective exponents κ that are collected in Table I, we see that errors in the 2D systems drop more rapidly than in the (harder) 3D systems. When expressed in terms of the total volume $N_{\rm sub} = L_{\rm sub}^d$, where d is the lattice dimension, this sharp change in the algebraic decays of errors between the 2D and 3D cases becomes yet more acute. In Ref. [28] (Sec. S13), we present scaling arguments that yield values of κ close to those that we observe numerically.

TABLE I. Parameters of the fits of the functional forms of Eqs. (2)–(4) to our data for the largest $L_{\rm sub}$ and L examined. The corresponding χ^2/d.o.f. values for Eqs. (2)–(4) are 0.821, 0.477, and 1.067 in 2D and 1.265, 0.794, and 0.656 in 3D, respectively. For the fit of the form (3) in 3D, we fixed $\beta = 1$. For the 2D systems, the form (2) was fitted with a cutoff $L_{\rm sub} \geq 16$ in order to minimize finite-size effects. The parameters $\ell_{\mathcal{E}}$ and κ of Eq. (2) are obtained by fitting the error rate as a function of $L_{\rm sub}$ at fixed $L = 1024$ in 2D and $L = 12$ in 3D. The parameters k_J, J, and β of Eq. (3) are obtained at fixed $L = 1024$ with $L_{\rm sub} = 64$ in 2D and at fixed $L = 12$ with $L_{\rm sub} = 10$ in 3D.

d	$\ell_{\mathcal{E}}$	κ	k_J	J
2D	0.20(1)	0.685(8)	0.198(8)	0.169(7)
3D	0.0006(10)	0.18(3)	0.47(3)	0.71(5)
d	β	ℓ_c	a_c	
2D	1.35(5)	1.01(3)	1.26(1)	
3D	1	1.40(9)	1.3(1)	

While the precise power-law decay differs between 2D and 3D, this variability is much less dramatic than the P vs NP computational complexity contrast between these cases. This observation suggests a "local hardness" computational complexity descriptor beyond the P-NP classification [19] (and related categories [41]), shedding further light on the intrinsic difficulty of spin-glass GS computations. By local hardness, we allude to how large the subsystem on which computations are done must be so that, when averaged over many instances, the local solver provides a correct answer up to a fixed error rate. Arguably, the local complexity is a relevant descriptor for physical local measurements (the microscopic state of the full many-body system cannot, in general, be probed).

For the case of nonzero average coupling $\bar{J}$, we find the same power-law decay as long as we remain in the (zero-temperature) spin-glass phase, thus suggesting some degree of universality in the behavior of local hardness. As soon as one enters the disordered ferromagnetic phase, however, there is a much faster, exponential decay of the error rate, cf. the data for $\bar{J} = 1.2$ in Fig. 2(a), Fig. 6 (End Matter), and further details in Ref. [28], Sec. S8. Similarly, we find identical 2D-type scaling and exponents for planar antiferromagnets having faint random perturbations of their couplings from an otherwise constant value (Ref. [28], Sec. S9). For the all-to-all SK model, on the other hand, the

data in Fig. 2(c) reveal that the local hardness does depend on the total system size N and not only on the $N_{\rm sub}$ randomly chosen spins forming the "local" subsystem, thus indicating a higher degree of local hardness of the SK model. This is consistent with the fact that there is no local geometry in the SK system, and that it consequently features a more complex free-energy landscape with infinitely many thermodynamic states [42]. As a result, one needs to scale $N_{\rm sub}$ proportionally to N to achieve a low error rate for the LSBS in the SK model.

We next turn to our central endeavor—that of understanding the physics underlying local solvers. Our approach relies on the concept of "critical thresholds" $J_{{\rm c},ij}$ [18,43], defined as follows. Across any bond, the spin product $\sigma_i\sigma_j$ is either $+1$ or -1. Consider now continuously varying J_{ij} from $-\infty$ to $+\infty$ leaving the strengths of all other bonds unchanged. As we have shown elsewhere [18], there is a unique value $J_{ij} = J_{{\rm c},ij}$ where the relative orientation of σ_i and σ_j changes from $\sigma_i = -\sigma_j$ ($J_{ij} < J_{{\rm c},ij}$) to $\sigma_i = \sigma_j$ ($J_{ij} > J_{{\rm c},ij}$) and, hence, two GSs become degenerate. A similar definition applies for the subsystem—changing the coupling J_{ij} beyond $J^{\rm sub}_{{\rm c},ij}$ leads to a change of the subsystem GS. For the LSBS we have the following important observation: If $J^{\rm sub}_{{\rm c},ij}$ and $J_{{\rm c},ij}$ are either (i) both smaller or (ii) both larger than J_{ij}, then the LSBS (determining the value of $\sigma_i\sigma_j$ as calculated within the smaller subsystem GS) will yield the correct $\sigma_i\sigma_j$ value (i.e., that computed within the global system GS). The opposite case of J_{ij} being sandwiched between $J_{{\rm c},ij}$ and $J^{\rm sub}_{{\rm c},ij}$, leading to a failure of LSBS, is more likely to occur if J_{ij} is close to the critical threshold. This is illustrated in Fig. 3, which correlates the error rate of bond predictions with the deviation of the couplings from criticality. Thus, the (subsystem) stability of a bond, captured by the distance $|J^{\rm sub}_{{\rm c},ij} - J_{ij}|$ between the bare coupling and its subsystem critical threshold, can serve as a predictor of LSBS reliability [44]. When $J^{\rm sub}_{{\rm c},ij}$ and J_{ij} are far apart, then $J^{\rm sub}_{{\rm c},ij}$ and $J_{{\rm c},ij}$ may indeed easily be both larger or both smaller than J_{ij}. Conversely, when $J^{\rm sub}_{{\rm c},ij}$ and J_{ij} are close, slight miscalculations can result in $J^{\rm sub}_{{\rm c},ij}$ and $J_{{\rm c},ij}$ appearing on opposite sides of J_{ij}, thus causing the LSBS to yield incorrect $\sigma_i\sigma_j$ values (see also Ref. [28], Sec. S3).

At the critical threshold $J_{{\rm c},ij}$, the GS responds sensitively to infinitesimal single-bond changes. Similar to avalanches in the random-field Ising model [45], neural networks [46], systems featuring highly optimized tolerance [47], and other problems [48], the GS spins that are flipped as a result of such changes form what we call zero energy droplets (ZEDs) featuring fractal boundaries and sizes conforming to power-law distributions [18]. In [28] (Sec. S13) we suggest a simple relation, which appears to be consistent with our data, that links ZED boundary Hausdorff dimensions to the exponent κ of Eq. (2). The ZED distributions and the heterogeneous

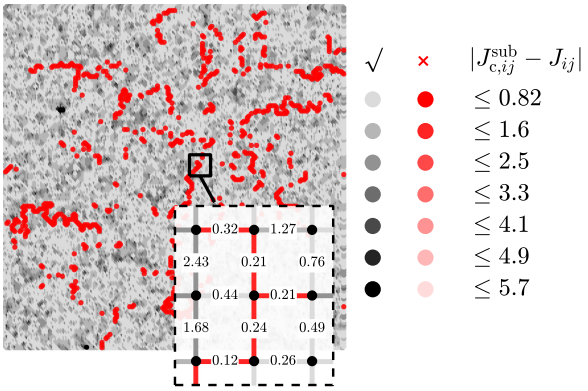


FIG. 3. LSBS solutions for nearest-neighbor bonds $\langle ij\rangle$ in an $L = 128$ system. An $L_{\rm sub} = 40$ subsystem is chosen to be centered about any such bond $\langle ij\rangle$ (near the boundaries, the subsystem becomes correspondingly smaller). $J^{\rm sub}_{{\rm c},ij}$ is the critical threshold of bond $\langle ij\rangle$. × denotes an error wherein the local solver does not match the global solution, while ✓ refers to correct LSBS predictions. Errors arise more readily for smaller $|J^{\rm sub}_{{\rm c},ij} - J_{ij}|$. It is noteworthy that correct LSBS predictions also appear for small values of $|J^{\rm sub}_{{\rm c},ij} - J_{ij}|$. Enlarged fragment: individual bond $|J^{\rm sub}_{{\rm c},ij} - J_{ij}|$ values are overlayed on color coded LSBS predictions for these bonds.

structure of these rare events, characterized by highly nonuniform spatial distributions, resemble the temperature-chaos [49–51] and disorder-chaos [17,51] phenomena in spin glasses, where rare events drive system-spanning changes. These distributions may be tied to complex critical spatial correlations (Ref. [28], Sec. S14). Configurations associated with general excitations may be constructed as composites of (single bond) ZEDs [18]. These excitations are, by construction, of vanishing energy. Near the critical threshold of a given bond, the global GS is extremely sensitive to infinitesimal changes of that local bond coupling, and the LSBS attains its lowest accuracy. However, when the coupling constants are sufficiently removed from their (measure zero) critical thresholds, the local solver becomes progressively more accurate. As is seen in Fig. 3 as well as in Fig. 4, End Matter, the error rate decays with increasing $|J^{\rm sub}_{{\rm c},ij} - J_{ij}|$. This decay is well described by

$$\mathcal{E}_{ij} \sim k_J e^{-\left(\frac{|J^{\rm sub}_{{\rm c},ij} - J_{ij}|}{\rm J}\right)^{\beta}}, \tag{3}$$

with $\beta > 1$ (2D) and $\beta = 1$ (3D), respectively, see Table I. As for the dependence on $L_{\rm sub}$ expressed in Eq. (2), the error rate $\mathcal{E}_{ij}$ exhibits the same functional dependence on the stability in 2D and 3D (Ref. [28], Sec. S7). The modulus $|J^{\rm sub}_{{\rm c},ij} - J_{ij}|$ is equal to twice the bond excitation energy ΔE within the subsystem, cf. Eq. (S1) in Ref. [28], Sec. S1. Thus, the LSBS accuracy is determined by this excitation energy.

We further tuned the central bonds of the $L = 128$ square and $L = 12$ cubic lattices to their critical values and computed the respective changes in critical threshold

($\Delta J_{c,ij}$) of all other bonds. We find that the average difference $|\Delta J_{c,ij}|$ decays algebraically with distance from the modified central bond (see Fig. 5, End Matter),

$$[|\Delta J_{c,ij}|] \sim (\ell_c/r)^{a_c}. \tag{4}$$

In 2D and 3D systems, both the length ℓ_c and the exponent a_c are of order unity, the fit parameters are provided in Table I. For sufficiently large r, the central bond coupling negligibly impacts the $J_{c,ij}$ of distant bonds. In other words, the critical coupling of a given bond is almost completely determined only by the couplings on bonds that are close to it. This exemplifies the "locality of the critical threshold $J_{c,ij}$." Since the ZED volume distribution decays algebraically [18], for large distances r between the tuned and observed bonds, the probability of ZED excitations connecting these bonds becomes small. When resampling the system boundary, $[|\Delta J_{c,ij}|]$ decays similar to Eq. (4), see Ref. [28], Sec. S10. Thus, generating a subsystem by removing peripheral bonds is of limited impact on the critical coupling of the central bond, thereby explaining the proximity of $J^{\mathrm{sub}}_{c,ij}$ and $J_{c,ij}$.

In summary, using exact GS algorithms, we study the effectiveness of divide-and-conquer type local subsystem solvers and relate it to critical threshold ZED physics [18] of system-spanning avalanchelike vanishing-energy excitations. In short-range spin glasses, away from critical thresholds, the response of the system GS to local perturbations decays rapidly. Generally, the difference between local and global minimization only becomes significant near critical coupling threshold values. Away from these critical values, local GS solvers achieve increased accuracy. Importantly, the associated error rate of the local solvers becomes independent of the system size [see Fig. 2(a)] for large systems and decreases rapidly with the subsystem size. Local solvers may thus become increasingly effective for large L. Our analysis reveals that various length-dependent quantities display algebraic scaling just like the scale-free distributions of avalanche size [18], while for ferromagnetic phases we observe an exponential decay of errors with subsystem size (see also End Matter and Ref. [28], Sec. S8). These behaviors may rationalize the success of more sophisticated solvers in spin glasses [24–26] and other systems [1,2], and might be broadly applicable in systems not constrained by the "overlap gap property" [52]. For the all-to-all SK model, on the other hand, the error rates always depend on the size of the full system. These differences lead us to conjecture a classification of possible levels of local hardness (Ref. [28], Sec. S6). Local solvers are found to be efficient for the studied lattices irrespective of whether the global problems are of P (2D) or NP (3D) complexity. The occurrence of rare events of bonds being close to their critical couplings explains why local solvers cannot, in general, guarantee finding the exact GSs of the full systems. This mechanism which is reminiscent of chaos in spin glasses [49–51] is generic for the classes of systems we study. It is instructive to briefly relate the local-hardness perspective to the metastate and chaotic-size-dependence framework [13], where one asks whether local observables have an effectively "concentrated" or more "dispersed" distribution over thermodynamic states. In our setting, large stability $|J^{\mathrm{sub}}_{c,ij} - J_{ij}|$ corresponds to a computable proxy for a robust metastatelike concentration of local observables of low LSBS error while small stability reflects competition between nearly degenerate states.

While these considerations were focused on the hyperlocal task of predicting the spins on both ends of a single bond, it is possible to stitch together the results of such calculations to candidate ground states of the full system. In the End Matter and Ref. [28] (Sec. S16), we outline an LSBS-based solver that uses the subsystem critical thresholds $J^{\mathrm{sub}}_{c,ij}$ to identify "well-determined" bonds, i.e., bonds for which $|J^{\mathrm{sub}}_{c,ij} - J_{ij}|$ is large and the LSBS error rate is exponentially small, cf. Eq. (3). This identification enables the contraction of the system into a smaller number of cohesive large-scale elements (or "communities" [53–56]) before solving for the GS. This extension is here presented as proof-of-concept demonstration of how local hardness can guide algorithm design, and further detailed study is required to gauge its full potential. Generalized to settings that include external fields and multibody interactions (Ref. [28], Sec. S15), our framework becomes applicable to other important NP-hard optimization problems, such as the minimum vertex cover problem (see End Matter and Ref. [28], Sec. S17). Locality further underlies numerous many-body physics problems [3–7] with continuous degrees of freedom. Replacing Eq. (1) by $H = -\sum_{\langle ij\rangle} J_{ij} s_i s_j + u \sum_i (s_i^2 - 1)^2$, with $u \gg 1$ and continuous $s_i \in \mathbb{R}$ [Eq. (1) is recovered as $u \to \infty$], suggests that our findings extend to continuous systems with sufficiently large quartic coupling u. In a continuous spin variant defined by a global constraint—the spherical model [57,58]—the locality that we described here is altered (Ref. [28], Sec. S12). Another interesting application area for the ideas outlined here lies in machine learning, with the potential of replacing slow global gradient methods by fast sequential local stochastic gradient descent-type approaches [55,56,59–62]. Local plastic variants of the backpropagation algorithm used in machine learning might emulate efficient biological neural computing [63,64]. Other notable aspects of local minimization and optimized structure appear in biological and artificial neural networks [65,66]. We view our LSBS-based contraction solver as a starting point for future investigations of local-hardness–guided heuristics. Dividing large-scale problems into smaller easier-to-solve fragments may also be beneficial for quantum computing schemes for which smaller-scale systems might suffer less from decoherence. Extensions of the GS problem analyzed here, including products between distant spins (see Ref. [28], Sec. S4) to finite temperature

correlation functions may provide illuminating connections between our results and Refs. [67–70]. In future work, we will further detail relations to previously unreported criticality (Ref. [28], Sec. S14). The physics of local optimization may underlie nature's efficiency, shaping computation across diverse realms.

Acknowledgments—We thank Mark Goh for a discussion in which he alerted us to [52]. Z. N. and M. W. are grateful for support from TU Chemnitz through the Visiting Scholar Program. Z. N. is further grateful for support through the Washington University Seeding Projects for Enabling Excellence & Distinction (SPEED) and the Leverhulme-Peierls Senior Researcher Professorship at Oxford via a Leverhulme Trust International Professorship Grant No. LIP2020-014 (S. L. Sondhi). G. O. gratefully acknowledges support from the Institute for Advanced Study.

Data availability—The data supporting the findings of this study are available from the authors upon reasonable request.

[1] A. Krizhevsky, I. Sutskever, and G. E. Hinton, Imagenet classification with deep convolutional neural networks, in *Advances in Neural Information Processing Systems (NeurIPS)*, edited by F. Pereira, C. J. Burges, L. Bottou, and K. Weinberger (Curran Associates, New York, 2012).
[2] J. Jumper *et al.*, Highly accurate protein structure prediction with AlphaFold, Nature (London) **596**, 583 (2021).
[3] W. Kohn, Density functional and density matrix method scaling linearly with the number of atoms, Phys. Rev. Lett. **76**, 3168 (1996).
[4] D. Ruelle, Cluster property of the correlation functions of classical gases, Rev. Mod. Phys. **36**, 580 (1964).
[5] E. H. Lieb and D. W. Robinson, The finite group velocity of quantum spin systems, Commun. Math. Phys. **28**, 251 (1972).
[6] B. Nachtergaele and R. Sims, Lieb-Robinson bounds and the exponential clustering theorem, Commun. Path. Phys. **265**, 119 (2006).
[7] M. Hastings and T. Koma, Spectral gap and exponential decay of correlations, Commun. Math. Phys. **265**, 781 (2006).
[8] B. A. Cipra, The Ising model is NP-complete, SIAM News **33**, 6 (2000).
[9] F. Barahona, On the computational complexity of Ising spin glass models, J. Phys. A **15**, 3241 (1982).
[10] M. Mezard, G. Parisi, and M. A. Virasoro, *Spin Glass Theory and Beyond* (World Scientific, Singapore, 1987).
[11] D. L. Stein and C. M. Newman, *Spin Glasses and Complexity* (Princeton University Press, Princeton, New Jersey, 2013).
[12] F. Menczer, S. Fortunato, and C. A. Davis, *A First Course in Network Science* (Cambridge University Press, Cambridge, England, 2020).
[13] M. Newman, *Networks: An Introduction* (Oxford University Press, Oxford, 2018), 2nd ed.
[14] J. D. Bryngelson and P. G. Wolynes, Spin glasses and the statistical mechanics of protein folding, Proc. Natl. Acad. Sci. U.S.A. **84**, 7425 (1987).
[15] Rugged Free Energy Landscapes—Common Computational Approaches to Spin Glasses, Structural Glasses and Biological Macromolecules, *Lect. Notes Phys.* edited by W. Janke (Springer, Berlin, 2007), Vol. 736.
[16] J. Lamarcq, J. P. Bouchaud, O. C. Martin, and M. Mézard, Non-compact local excitations in spin-glasses, Europhys. Lett. **58**, 321 (2002).
[17] F. Krzakala and J.-P. Bouchaud, Disorder chaos in spin glasses, Europhys. Lett. **72**, 472 (2005).
[18] M. Shen, G. Ortiz, Y.-Y. Liu, M. Weigel, and Z. Nussinov, Universal fragility of spin-glass ground states under single bond changes, Phys. Rev. Lett. **132**, 247101 (2024).
[19] C. H. Papadimitriou, *Computational Complexity* (Addison-Wesley, Reading, MA, 1994).
[20] L. Bieche, J. P. Uhry, R. Maynard, and R. Rammal, On the ground-states of the frustration model of a spin-glass by a matching method of graph-theory, J. Phys. A **13**, 2553 (1980).
[21] S. F. Edwards and P. W. Anderson, Theory of spin glasses, J. Phys. F **5**, 965 (1975).
[22] D. Sherrington and S. Kirkpatrick, Solvable model of a spin-glass, Phys. Rev. Lett. **35**, 1792 (1975).
[23] B. Sun, B. Leonard, P. Ronhovde, and Z. Nussinov, An interacting replica approach applied to the traveling salesman problem, *2016 SAI Computing Conference* (IEEE, New York, 2016), p. 319.
[24] W. Wang, S. Mandrà, and H. G. Katzgraber, Patch-planting spin-glass solution for benchmarking, Phys. Rev. E **96**, 023312 (2017).
[25] C. Fan, M. Shen, Z. Nussinov, Z. Liu, Y. Sun, and Y.-Y. Liu, Finding spin glass ground states through deep reinforcement learning, Nat. Commun. **14**, 725 (2023).
[26] C. Fan, M. Shen, Z. Nussinov, Z. Liu, Y. Sun, and Y.-Y. Liu, Reply to: Deep reinforced learning heuristic tested on spin-glass ground states: The larger picture, Nat. Commun. **14**, 5659 (2023).
[27] A. K. Hartmann and A. P. Young, Metastate analysis of the ground states of two-dimensional Ising spin glasses, Phys. Rev. E **108**, 024142 (2023).
[28] See Supplemental Material at http://link.aps.org/supplemental/10.1103/kcbw-6zkv for scaling arguments, extended numerical fits, contraction-solver details, multibody correlations, MVC mapping, and additional model studies, which includes Refs. [29–35].
[29] G. H. Wannier, Antiferromagnetism. The triangular Ising net, Phys. Rev. **79**, 357 (1950).
[30] J. Villain, Spin glass with non-random interactions, J. Phys. C **10**, 1717 (1977).
[31] M. E. Fisher, Statistical mechanics of dimers on a plane lattice, Phys. Rev. **124**, 1664 (1961).
[32] M.-S. Vaezi, G. Ortiz, M. Weigel, and Z. Nussinov, The binomial spin glass, Phys. Rev. Lett. **121**, 080601 (2018).
[33] A. Lucas, Ising formulations of many NP problems, Front. Phys. **2**, 5 (2014).
[34] J. Chen, L. Kou, and X. Cui, An approximation algorithm for the minimum vertex cover problem, Procedia Eng. **137**, 180 (2016).
[35] J. Chen, R. Zhou, J. Wu, H. Zhang, and W. Gui, Vertex cover of networks and its related optimization problems: An

overview, IEEE Trans. Neural Networks Learn. Syst. **36**, 11738 (2024).
[36] H. Khoshbakht and M. Weigel, Domain-wall excitations in the two-dimensional Ising spin glass, Phys. Rev. B **97**, 064410 (2018).
[37] V. Kolmogorov, Blossom V: A new implementation of a minimum cost perfect matching algorithm, Math. Program. Comput. **1**, 43 (2009).
[38] Gurobi Optimization, LLC, Gurobi Optimizer Reference Manual, 2022.
[39] While we will largely focus on the central nearest neighbor bond (with $i = i_0$ and $j = j_0$), in the End Matter we discuss more general situations in which the sites i and j are a distance $r_{ij} > 1$ apart. In order to avoid cumbersome notation, in the main text, we will often dispense with "0" subscripts.
[40] For the largest values of $L_{\mathrm{sub}} = \mathcal{O}(L)$, the right-hand side of Eq. (2) constitutes an upper bound on the error $\mathcal{E}_{ij}$. Clearly, when $L_{\mathrm{sub}} = L$ (when the subsystem is the entire system), the error $\mathcal{E}_{ij} = 0$ by definition.
[41] M. Yannakakis, Equilibria, fixed points, and complexity classes, Comput. Sci. Rev. **3**, 71 (2009).
[42] G. Parisi, Infinite number of order parameters for spin-glasses, Phys. Rev. Lett. **43**, 1754 (1979).
[43] C. M. Newman and D. L. Stein, Ground state stability and the nature of the spin glass phase, Phys. Rev. E **105**, 044132 (2022).
[44] A very similar behavior is observed for the distance $|J_{c,ij} - J_{ij}|$, see the discussions in Supplemental Material Sec. S10, but this quantity is not accessible from the perspective of the local solver.
[45] J. P. Sethna, K. A. Dahmen, and C. R. Myers, Crackling noise, Nature (London) **410**, 242 (2001).
[46] A. Klaus, S. Yu, and D. Plenz, Statistical analyses support power law distributions found in neuronal avalanches, PLoS One **6**, e19779 (2011).
[47] J. M. Carlson and J. Doyle, Highly optimized tolerance: Robustness and design in complex systems, Phys. Rev. Lett. **84**, 2529 (2000).
[48] V. Navas-Portella, I. Serra, A. Corral, and E. Vives, Increasing power-law range in avalanche amplitude and energy distributions, Phys. Rev. E **97**, 022134 (2018).
[49] L. Fernandez, V. Martin-Mayor, G. Parisi, and B. Seoane, Temperature chaos in 3D Ising spin glasses is driven by rare events, Europhys. Lett. **103**, 67003 (2013).
[50] M. Baity-Jesi *et al.*, Temperature chaos is present in off-equilibrium spin-glass dynamics, Commun. Phys. **4**, 74 (2021).
[51] H. G. Katzgraber and F. Krzakala, Temperature and disorder chaos in three-dimensional Ising spin glasses, Phys. Rev. Lett. **98**, 017201 (2007).
[52] D. Gamarnik, The overlap gap property: A topological barrier to optimizing over random structures, Proc. Natl. Acad. Sci. U.S.A. **118**, e2108492118 (2021).
[53] M. Girvan and M. E. J. Newman, Community structure in social and biological networks, Proc. Natl. Acad. Sci. U.S.A. **99**, 7821 (2002).
[54] Santo Fortunato, Community detection in graphs, Phys. Rep. **486**, 75 (2010).
[55] P. Ronhovde and Z. Nussinov, Multiresolution community detection for mega-scale networks by information-based replica correlations, Phys. Rev. E **80**, 016109 (2009).
[56] P. Ronhovde and Z. Nussinov, Local resolution-limit-free model for community detection, Phys. Rev. E **81**, 046114 (2010).
[57] T. H. Berlin and M. Kac, The spherical model of a ferromagnet, Phys. Rev. **86**, 821 (1952).
[58] J. M. Kosterlitz, D. J. Thouless, and R. C. Jones, Spherical model of a spin glass, Physica B+C (Amsterdam) **86–88**, 859 (1977).
[59] A. Harju, B. Barbiellini, S. Siljamäki, R. M. Nieminen, and G. Ortiz, Stochastic gradient approximation: An efficient method to optimize many-body wave functions, Phys. Rev. Lett. **79**, 1173 (1997).
[60] S. Ruder, An overview of gradient descent optimization algorithms, 2016, arXiv:1609.04747.
[61] L. Bottou, F. E. Curtis, and J. Nocedal, Optimization methods for large-scale machine learning, SIAM Rev. **60**, 223 (2018).
[62] K. Choudhary *et al.*, Recent advances and applications of deep learning methods in materials science, npj Comput. Mater. **8**, 59 (2022).
[63] Y. Song, T. Lukasiewicz, Z. Xu, and R. Bogacz, Can the brain do backpropagation? Exact implementation of backpropagation in predictive coding networks, in Advances in Neural Information Processing Systems (NeurIPS), edited by H. Larochelle, M. Ranzato, R. Hadsell, M. F. Balcan, and H. Lin (Curran Associates, New York, 2020).
[64] I. Goodfellow, Y. Bengio, and A. Courville, *Deep Learning* (MIT Press, Cambridge, MA, 2016).
[65] F. Alet, T. Lozano-Perez, and L. P. Kaelbling, Modular meta-learning, In *2nd Conference on Robot Learning (CoRL)*, (Zurich, Switzerland, 2018).
[66] D. Meunier, R. Lambiotte, and E. T. Bullmore, Modular and hierarchically modular organization of brain networks, Front. Neurosci. **4**, 200 (2010).
[67] D. A. Huse and I. Morgenstern, Finite-size scaling study of the two-dimensional Ising spin glass, Phys. Rev. B **32**, 3032 (1985).
[68] A. C. Carter, A. J. Bray, and M. A. Moore, On the use of finite-size scaling to measure spin-glass exponents, J. Phys. A **36**, 5699 (2003).
[69] F. Parisen Toldin, A. Pelissetto, and E. Vicari, Finite-size scaling in two-dimensional Ising spin glass models, Phys. Rev. E **84**, 051116 (2011).
[70] T. Aspelmeier, H. G. Katzgraber, D. Larson, M. A. Moore, M. Wittmann, and J. Yeo, Finite-size critical scaling in Ising spin glasses in the mean-field regime, Phys. Rev. E **93**, 032123 (2016).
[71] We emphasize that the collected data and their fits were for the finite values of $|J^{\mathrm{sub}}_{c,ij} - J_{ij}|$ shown in the figure. When $J^{\mathrm{sub}}_{c,ij} \neq J_{c,ij}$, the error rate $\mathcal{E}_{ij} \to 1/2$ as $|J^{\mathrm{sub}}_{c,ij} - J_{ij}| \to 0^+$, while coincident thresholds $J^{\mathrm{sub}}_{c,ij} = J_{c,ij}$ (as invariably occurs in the open 1D chain) yield zero error in this limit. At exact GS degeneracy, numerical solvers need not sample both GSs equally. For the finite abscissa values in Fig. 4, the 3D data lies closer to $1/2$ than the 2D data.
[72] O. Melchert and A. K. Hartmann, Scaling behavior of domain walls at the zero-temperature ferromagnet to spin-glass transition, Phys. Rev. B **79**, 184402 (2009).

End Matter

Here, we provide numerical evidence for Eqs. (3) and (4), the existence of a transition in the LSBS accuracy as the distribution of couplings is shifted (so as to make the system more ferromagnetic and easier to solve), and we discuss beyond nearest-neighbor correlations found by the LSBS.

Error rates for deviations from the critical threshold—Illustrating the applicability of the analysis in the main text, Fig. 4 demonstrates that the LSBS error indeed decays with increasing $|J^{\mathrm{sub}}_{\mathrm{c},ij} - J_{ij}|$ in a manner that adheres to the stretched exponential drop of Eq. (3) [71].

Distance dependence of critical threshold values—As discussed in the main text, the critical threshold of a given bond is largely determined only by the couplings of other bonds that are very close to it. When we tune the central bonds of $L = 128$ square and $L = 12$ cubic lattices to their critical values, the respective critical threshold changes ($\Delta J_{\mathrm{c},ij}$) of all other bonds at a distance r conform to Eq. (4), where ℓ_c is of the order of the lattice constant, see Table I [with the fit of Eq. (4) becoming an upper bound for the largest distances in the 2D system]. This is illustrated in Fig. 5. In Ref. [28], Sec. S5 (see Fig. S4 therein), we further provide a calculated real-space visualization of such a typical rapid drop of the change in the critical coupling away from the origin. We further observe a smaller effect on distant bonds for smaller ZEDs.

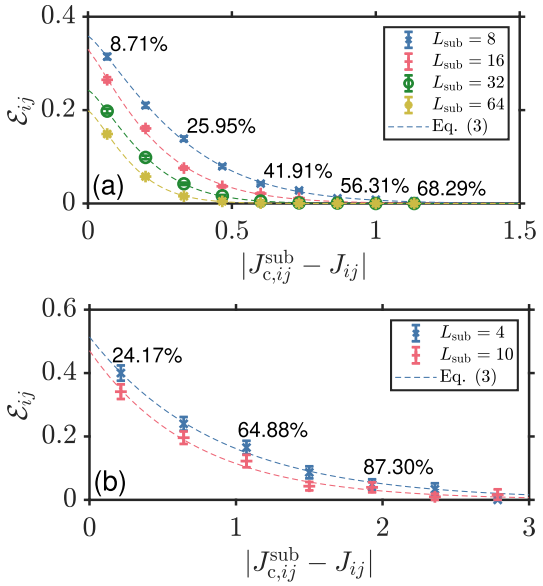


FIG. 4. Error rate $\mathcal{E}_{ij}$ as a function of $|J^{\mathrm{sub}}_{\mathrm{c},ij} - J_{ij}|$ for (a) a 2D (square lattice), $L = 1024$ system with $L_{\mathrm{sub}} = 8$, 16, 32, 64 and (b) a 3D (cubic) system of $L = 12$ with $L_{\mathrm{sub}} = 4$, 10. Point percentages denote cumulative probabilities (i.e., fraction of instances) for values of $|J^{\mathrm{sub}}_{\mathrm{c},ij} - J_{ij}|$ lower than their abscissa.

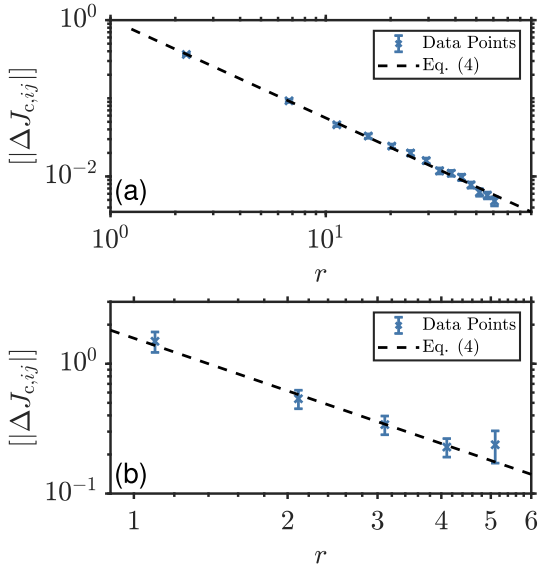


FIG. 5. Average change of critical threshold values ($[|\Delta J_{\mathrm{c},ij}|]$) of bonds a distance r along a Cartesian direction away from the central bond in (a) 2D ($L = 128$) and (b) 3D ($L = 12$) systems. Dashed line: Eq. (4) with parameters in Table I. As is more evident in 2D, when $r = \mathcal{O}(L)$, the average $[|\Delta J_{\mathrm{c},ij}|]$ is bounded from above by these ultra-local forms with the fitted ℓ_c being of the order of the lattice constant.

Contraction solver based on LSBS—The LSBS provides local predictions for individual nearest-neighbor bond spin products. Here we outline how these local predictions can be combined into a *contraction solver* that approximates the full GS spin configuration. For each bond, we compute its subsystem critical threshold

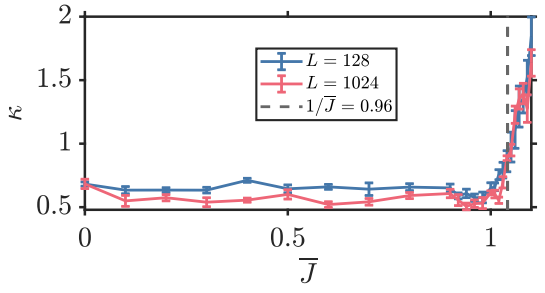


FIG. 6. For an asymmetric bond distribution, as $\bar{J}$ increases the system transitions from a spin-glass phase to a disordered ferromagnetic phase [72]. We observe how the fitting coefficient κ changes as we adjust $\bar{J}$. A larger value of κ implies that the error rate of the subsystem solver decays faster, with a crossover to an exponential decay beyond the threshold $1/\bar{J} = 0.96$, where the system enters the ferromagnetic phase [72].

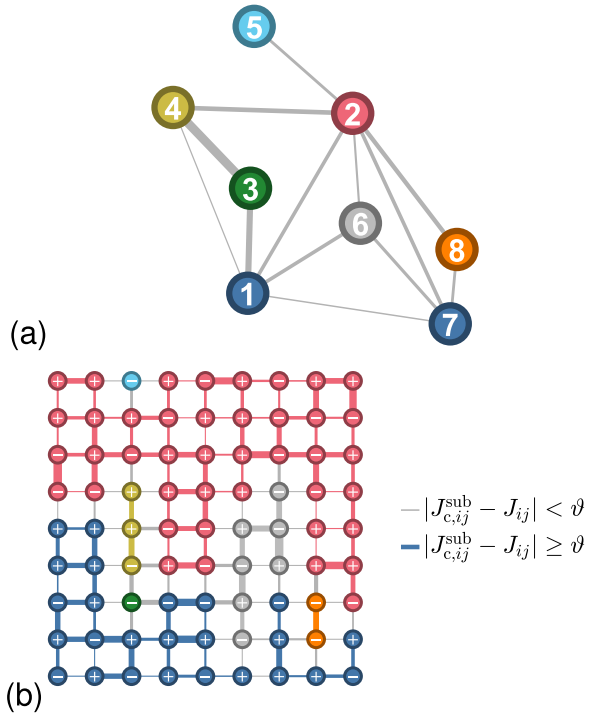


FIG. 7. Schematic of the contraction solver. (a) Well-determined bonds ($|J_{ij} - J_{\mathrm{c},ij}| \geq \vartheta$, where ϑ is a manually chosen threshold) form connected components that are contracted to effective sites (shown as larger nodes), inheriting all interactions between the component and the rest of the system. (b) The relative spin orientations (indicated by + and − signs) of sites within each connected component are locked in by the well-determined bonds. The GS of the full system can then be reconstructed from the GS of the contracted system by propagating the component orientations. Different colors represent distinct connected components.

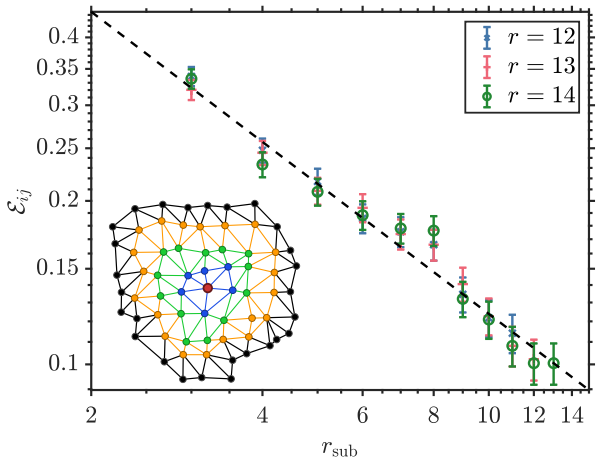


FIG. 8. Minimum vertex cover (MVC) as an Ising problem on random planar graphs. LSBS error rate for the central spin in the MVC mapping, of the random planar graph shown in the inset, as a function of subsystem size, showing a power-law-like decay with exponent $\kappa \approx 0.8$. (Lower left inset) Random planar graph generated from $n = 10^4$ points by Delaunay triangulation, with sites colored by topological distance r from the geometric center.

$J_{\mathrm{c},ij}$ and identify well-determined bonds satisfying $|J_{ij} - J_{\mathrm{c},ij}| \geq \vartheta$, where ϑ is a chosen threshold. These bonds, being far from their critical thresholds, have high local prediction accuracy. Well-determined bonds form connected components (or "communities" [53–56]) within which relative spin orientations are reliably fixed. Each such component is contracted to a single effective site, inheriting all interactions between the component and the rest of the system. The contracted system is solved exactly, and the original spin configuration is reconstructed by propagating the component orientations. This contraction procedure is illustrated schematically in Fig. 7. For appropriate choices of ϑ, this approach yields configurations very close to the exact GS while substantially reducing the effective problem size. Detailed schematics, algorithmic steps, and a performance analysis are provided in Supplemental Material (Ref. [28], Sec. S16).

Minimum vertex cover as an Ising problem—As a representative NP-hard optimization problem beyond spin glasses, we also examined the minimum vertex cover (MVC) problem on random planar graphs generated by Delaunay triangulation. By mapping a vertex i in the cover to $\sigma_i = +1$ and $\sigma_i = -1$ otherwise, the cost function can be written as

$$H_{\mathrm{MVC}} = A\sum_{i\in V}\frac{1+\sigma_i}{2} + B\sum_{\langle ij\rangle\in E}\frac{1-\sigma_i}{2}\frac{1-\sigma_j}{2}, \qquad \text{(D1)}$$

with couplings $J_{ij} = -B/4$ on edges $\langle ij\rangle \in E$ and fields $h_i = -A/2 + (B/4)\deg(i)$ (for $A = 1$, $B = 2$), where $\deg(i)$ corresponds to the degree (number of neighbors) of site i. Using LSBS on subsystems of graph distance radius r around a central site, we predict its relative spin orientation in the MVC GS and compare that to the exact solution. We find a power-law-like decay of the LSBS error rate with subsystem size (Fig. 8), with exponent $\kappa \approx 0.8$, close to that of the spin-glass case. This suggests that our locality-based hardness picture applies more broadly to combinatorial optimization problems.